Proceedings of the International Conference on Oxide Materials for Electronic Engineering (OMEE 2021)

Synthesis, Phase Transformations of Polymorphous Nanooxidic Forms of Iron and Their Interaction with Sulfur Dioxide

T.L. Rakitskaya, A.S. Truba*,
A.P. Nazar and T.A. Kiose

Faculty of Chemistry and Pharmacy, Odessa I.I. Mechnikov National University, 2, St. Dvoryanskaya, 65082 Odessa, Ukraine

Doi: 10.12693/APhysPolA.141.281 *e-mail: tlr@onu.edu.ua

Monophase iron oxide samples (α-Fe_2O_3, γ-Fe_2O_3, and α-FeO(OH)) and also mixtures of iron oxides with different phase compositions, i.e., Fe_3O_4, γ-FeO(OH), α-FeO(OH), and α-FeO(OH), α-Fe_2O_3, were obtained by a precipitation method with variable nature of iron salts, precipitators as well as drying and calcination temperatures. The samples were identified by XRD, SEM, and FT-IR spectroscopy methods. The samples were also tested in the reaction with sulfur dioxide at an initial SO_2 concentration in the gas-air mixture of 150 mg/m^3, a gas-air mixture volume flow rate of 16.6 cm^3/s, the relative humidity of 76%, and a temperature of 20°C. Interaction of SO_2 with iron(III) nanooxides in the air does not result in the formation of new phases. The FT-IR spectra give evidence of the formation of surface sulfite and bisulfite forms from SO_2 adsorbed.

topics: iron(III) oxide, nanooxide, phase transformation, sulfur dioxide

1. Introduction

Iron(III) nanooxides (α-Fe_2O_3, γ-Fe_2O_3, Fe_3O_4, α-FeO(OH) and β-FeO(OH)) catalyze many redox reactions, including ozone decomposition [1–5] and oxidation of sulfur dioxide [6–13]. Analysis of the literature showed that considerable attention is paid to the interaction of SO_2 with oxide forms of iron in the aerosol cycle of the atmosphere [7, 8]. Photocatalytic oxidation of SO_2 on powders of some semiconductors was studied by the authors in [9, 10], and the following series of activities have been established: $Fe_2O_3 \sim ZnO \sim CdS \sim TiO_2$ [10]. The rate of SO_2 photooxidation in the presence of polymorphic forms of iron oxide changes within two orders of magnitude in the series: γ-FeO(OH) > α-Fe_2O_3 > γ-Fe_2O_3 > δ-FeO(OH) > β-FeO(OH) > α-FeO(OH) [11]. Heterogeneous reactions of SO_2 on typical mineral materials are irreversible and proceed with the formation of sulfo- (SO_3^{2-}), bisulfite- (HSO_3^-), and sulfate- (SO_4^{2-}) ions. The reactivity of these materials decreases in the following sequence: FeO(OH) > Al_2O_3 > MgO > TiO_2 > Fe_2O_3 > SiO_2 [12]. A spectroscopic study of the adsorption and oxidation of SO_2 on iron oxides at room temperature gives the following sequence of reactivity: α-Fe_2O_3 > γ-Fe_2O_3 > Fe_3O_4 > β-FeO(OH) > α-FeO(OH) [13].

From the data presented, it can be concluded that the position in the activity series of polymorphic forms of iron oxides is ambiguous [11, 13], and in some cases [10, 12] the polymorphic type is not specified.

There are no systematic studies of the effect of the structural and morphological properties of polymorphic forms of iron(III) oxides on the kinetics of SO_2 oxidation by atmospheric oxygen and the time of protective action, which complicates the targeted synthesis of such materials for practical use in order to protect the environment from the harmful effects of the most common air pollutant.

The objective of this work is to synthesize iron(III) nanooxides by various methods to establish the structure and morphology of the samples and their effect on the kinetic parameters of the reaction, namely the time of the protective action and the specific amount of reacted sulfur dioxide.

2. Experimental

Several series of IS-Fe–VS-Fe samples were obtained by the precipitation method by varying the nature of iron(II) and iron(III) salts, precipitant, drying and calcination temperatures, including monophase α-Fe_2O_3, γ-Fe_2O_3, α-FeO(OH), as well as mixtures of different compositions

TABLE I

Samples of iron oxides used in the work.

No.	Name of sample	The brief method description	Ref.
1	IS-Fe-200	precipitation method; reagents $FeCl_3$, $FeSO_4$ and 25% water solution NH_3; solution was left for 72 h; precipitants were dried at 200°C for 5 h;	[5]
2	IS-Fe-500	the precursor as in line 1 was calcined at 500 °C for 3 h;	–
3	IIS-Fe-200	reagents $Fe_2(SO_4)_3 \cdot 9H_2O$, $FeSO_4 \cdot 7H_2O$ and NH_4OH; the synthesis sequence as in line 1;	[5]
4	IIS-Fe-300	the precursor as in line 3 was calcined at 300°C for 3 h;	–
5	IIS-Fe-500	the precursor as in line 3 was calcined at 500°C for 3 h;	–
6	IIIS-Fe-110	hydrogel method; reagents $FeSO_4$ and NH_4OH; the gel was refluxed for 4 h in N_2 stream; dried at 110°C;	[14]
7	IVS-Fe-20 IVS-Fe-110 IVS-Fe-200 IVS-Fe-300 IVS-Fe-500	precipitation method; reagents $Fe(NO_3)_3 \cdot 9H_2O$, NH_4OH; the precipitate was treated with concentrated KOH solution and water vapor; the precipitate was dried at 20 and 110°C and calcined at 200, 300, 500°C;	[15]
8	VS-Fe-110	reagents $Fe(NO_3)_3 \cdot 9H_2O$, glycerin, urea; the solution was heated at 110°C for 12 h; the precipitate was dried at 110°C;	[16]
9	VS-Fe-500	the precursor as in line 8 was calcined at 500°C	–

— Fe_3O_4, γ-FeO(OH), α-FeO(OH) and α-Fe_2O_3, α-FeO(OH). The reference designation of the samples and a brief description of the methods of their preparation are summarized in Table I. The samples were identified by XRD, SEM, and FT-IR spectroscopy according to the methods [6] and tested in reaction with SO_2.

The gas-air mixture (GAM) with SO_2 concentration of 150 mg/m^{3}was obtained by mixing a purified airflow and a flow of pure SO_2 in a special mixer. The initial ($C^{\text{in}}_{SO_2}$) and final ($C^{\text{f}}_{SO_2}$) sulfur dioxide concentrations were measured using a 667EKh08 electrochemical gas analyzer (made by "Analitpribor", Ukraine) with minimal detectable SO_2 concentration of 2 mg/m^3.

The kinetics of sulfur dioxide oxidation with air oxygen over catalytic compositions was investigated using a gas flow setup with a fixed-bed reactor thermostated at 293 K, with the relative humidity of the GAM φ_{GAM} kept at 76%. The weight of each studied sample was 0.5 g. The volume flow rate w of the GAM (1 L/min), the linear velocity U of the GAM (6.2 cm/s), and the ratios between the average grain size and geometric parameters of the reactor met the requirements for the regime of ideal displacement and the reaction proceeding in the kinetic region.

3. Results and discussion

3.1. Phase composition

The diffractograms of some samples are shown in Fig. 1 as an example. It follows from the diffraction patterns that all samples, except for VS-Fe-110, are crystalline. However, the number and positions of reflections, as well as their intensities, depend on the nature of iron precursors, production process, and calcination temperature. The initial search-match procedure let us identify the following phases: hematite, α-Fe_2O_3 (JCPDS 33-0664), maghemite, γ-Fe_2O_3 (JCPDS 39-1346), magnetite, Fe_3O_4 (JCPDS 19-0629), and goethite, α-FeO(OH) (JCPDS 29-0713). The quantitative phase analysis for samples was carried out using the Rietveld method. From the results of calculations shown in Table II, the following conclusions can be drawn. Samples IIS-Fe-300, IVS-Fe-20, and IVS-Fe-110 are monophasic. All samples calcined at 500°C contain only the α-Fe_2O_3 phase. Samples IIIS-Fe-110 and IVS-Fe-200 are polyphase. Sample VS-Fe-110 is semi-morphic, in which it is impossible to unambiguously determine the phase composition. Upon calcination, a phase transformation occurs, and crystalline α-Fe_2O_3 (hematite) is formed. The diffractogram of the hematite sample after interaction with SO_2 (Fig. 1f) is similar to the diffractogram of the initial sample. Calculations by the Rietveld method (Table II) showed the presence of only the hematite phase (α-Fe_2O_3) and a decrease in the size of the crystallites of this phase after reaction with SO_2 to 57 nm. The Fe_3O_4 and α-Fe_2O_3 phases have the largest crystallite size. For the VS-Fe-500 sample, the crystallite size decreases after the reaction with sulfur dioxide.

3.2. FT-IR spectroscopy

IR spectra of monophase samples γ-Fe_2O_3, α-FeO(OH), α-Fe_2O_3, and a polyphase sample containing Fe_3O_4, α-FeO(OH), and γ-FeO(OH) are in accordance with the data [17] and are described in our works [4, 5].

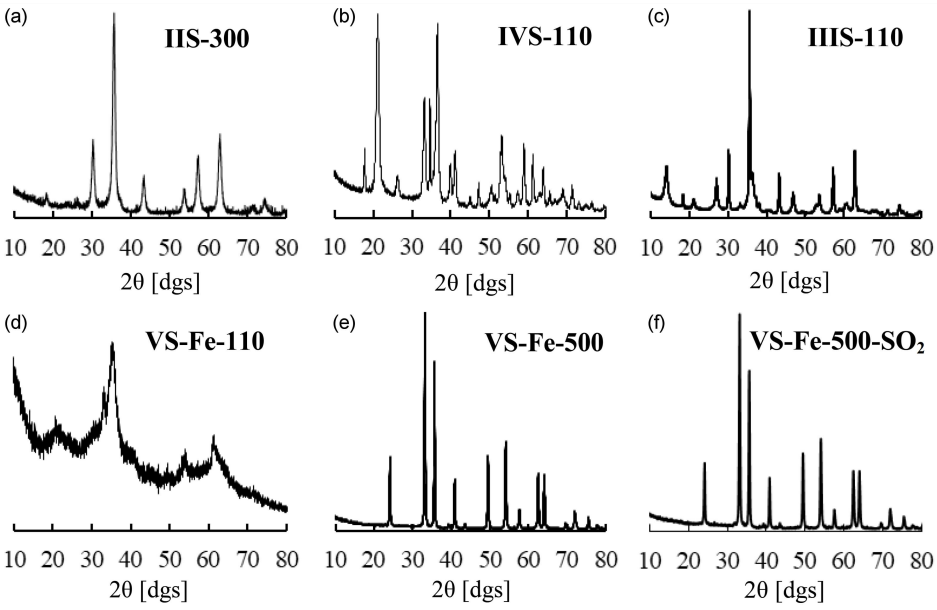

Fig. 1. X-ray diffraction patterns of initial samples: (a) — IIS-300 (γ-Fe_2O_3); (b) — IVS-110 (α-FeO(OH)); (c) — IIIS-110 (Fe_3O_4, γ-FeO(OH), α-FeO(OH)); (d) — VS-Fe-110 (semi-amorphous); (e) — VS-Fe-500 (α-Fe_2O_3) and a sample with a reaction with SO_2: (f) — VS-Fe-500–SO_2(α-Fe_2O_3).

The results of identification of the IR spectra (not shown) of the initial hematite samples obtained on the basis of various precursors (Table I) and after their interaction with sulfur dioxide are summarized in Table III. It should be noted that in the spectra of samples IVS-Fe-500–SO_2 and VS-Fe-500–SO_2, two new bands appear at 1138 and 1040 cm^{-1}, which, according to [18], we attribute to the oscillations of the S–O bond in mono- and bidentate surface sulfite complexes. In the case of the IVS-Fe-500–SO_2 sample, a shift of the absorption bands of the Fe–O bond (ν_{Fe-O}) is observed in the region of larger values of the wave numbers. Minor changes in ν_{Fe-O} are observed in the spectrum of the sample VS-Fe-500–SO_2.

3.3. Morphology

The synthesized samples of IS-Fe–VS-Fe demonstrated a variety of morphotypes, which is consistent with many literature data [19, 20]. In this work, we present SEM images of VS-Fe-110 (Fig. 2a–b) and VS-Fe-500 (Fig. 2c–d) samples before and after their interaction with sulfur dioxide. These samples, according to the results of their testing in the reaction with SO_2, absorbed the largest amount of SO_2 moles. The surface of the semi-amorphous sample VS-Fe-110 is characterized by an inhomogeneous morphology. These are mainly "hedgehog-like" spheres, which are formed from acicular crystallites and lamellar agglomerates (Fig. 2a). After the interaction with SO_2, the surface morphology of the VS-Fe-110 sample is mainly retained. However, on the surface of agglomerates, which are composed of acicular crystallites, fine crystalline particles appear (Fig. 2b).

TABLE II

Phase composition and phase parameters in the case of iron oxide samples.

Sample	Phase	Content of the phase [wt%]	Size of the crystallites [nm]
IS-Fe-200	α-Fe_2O_3	57.0	6
	Fe_3O_4	11.5	8
	γ-Fe_2O_3	15.7	8
	α-FeO(OH)	15.7	11
IS-Fe-500	α-Fe_2O_3	100.0	16
IS-Fe-200	γ-Fe_2O_3	100.0	7.2
IIS-Fe-300	γ-Fe_2O_3	100.0	7.4
IIS-Fe-500	α-Fe_2O_3	100.0	38
IIIS-Fe-110	Fe_3O_4	49.6	38
	γ-FeO(OH)	39.1	11.3
	α-FeO(OH)	9	9
IVS-Fe-20	α-FeO(OH)	100.0	15
IVS-Fe-110	α-FeO(OH)	100.0	15
IVS-Fe-200	α-FeO(OH)	78.7	15
	α-Fe_2O_3	21.3	6
IVS-Fe-300	α-Fe_2O_3	100.0	11
IVS-Fe-500	$\alpha-Fe_2O_3$	100.0	30
VS-Fe-110	semi-amorphous mixture	–	–
VS-Fe-500	$\alpha-Fe_2O_3$	100.0	64
VS-Fe-500–SO_2	$\alpha-Fe_2O_3$	100.0	57

Sample VS-Fe-500 was obtained by calcination of sample VS-Fe-110 for 3 h. According to X-ray diffraction (Table II), it contains only the hematite phase α-Fe_2O_3 (100%). Against the background of a chaotic plexus of needle crystallites with a width

TABLE III

Wave numbers (ν [cm^{-1}]) of absorption maxima in the IR spectra of the samples.

Sample	ν_{OH}	δ_{H_2O}	ν_{Fe-O}	ν_{Fe-OH}	ν_{S-O} (sulfite group)
IVS-Fe-500	3383	1631	513; 426; 415; 410	910	–
IVS-Fe-500-SO_2	3383	1631	515; 430; 422; 416	916	1138; 1040
VS-Fe-500	3393	1644	513; 429; 426	–	–
VS-Fe-500–SO_2	3392	1644	513; 426; 422	–	1136; 1040

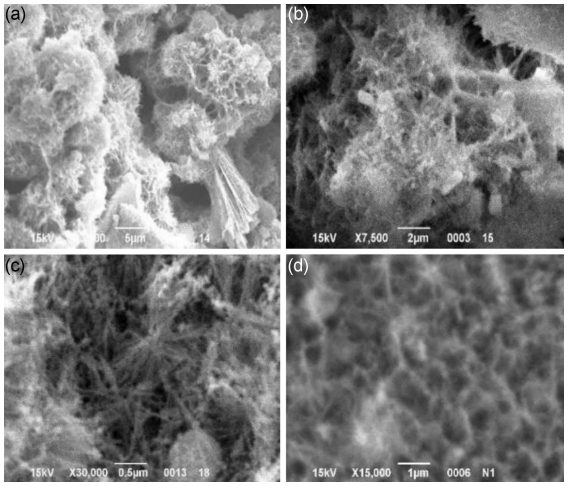

Fig. 2. SEM image of the surface of the sample VS-Fe-110 (a, b) and VS-Fe-500 (c, d) before (a, c) and after (b, d) reaction with sulfur dioxide.

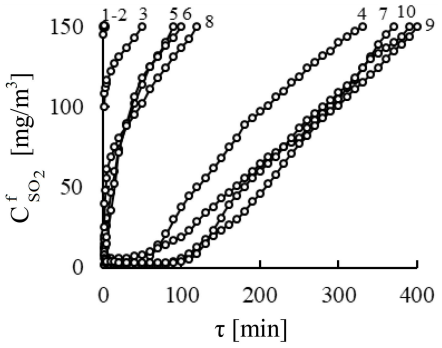

Fig. 3. The change in $C^f_{SO_2}$ over time in the reaction of sulfur dioxide with samples of oxide forms of iron obtained in different ways. (The numbers of the curves correspond to the numbering in Table IV.) ($C^{in}_{SO_2}$ = 150 mg/m^3; m = 0.5 g; U = 10.2 cm/s; temperature of T = 20°C.

of ≈ 20 and a length of up to 2000 nm, a melon-like formation is well defined (Fig. 2c). It also is formed by a plexus of needle crystallites. After interaction of VS-Fe-500 with sulfur dioxide the surface morphology of the sample is inhomogeneous and undergoes some changes.

3.4. Testing of iron oxide samples in reaction with sulfur dioxide

The kinetic curves that characterize the time change of the concentration of SO_2 in the GAM at the outlet of the reactor are shown in Fig. 3. It is seen that the profiles of the kinetic curves depend on the phase composition of the samples. There are three groups of samples. The first group of samples, i.e., IS-Fe-500 (curve 1), IIS-Fe-300 (curve 2), and IIS-Fe-500 (curve 3), practically does not react with sulfur dioxide. The second group of samples, i.e., IVS-Fe-20 (curve 5), IVS-Fe-110 (curve 6), and IVS-Fe-500 (curve 8) is inactive. The final concentration of SO_2 ($C^f_{SO_2}$) for these samples increases rapidly and reaches the initial concentration of SO_2 almost for the same period of time. The third group of samples, i.e., IIIS-Fe-110 (curve 4), IVS-Fe-200 (curve 7), VS-Fe-110 (curve 9), and VS-Fe-500 (curve 10), is the most active as the samples show kinetics. Namely, at the initial site for some time $C^f_{SO_2} < MPC_{SO_2}$ (10 mg/m^3), which corresponds to the time of protective action of the sample (τ_{MPC}), and then the concentration of SO_2 increases, and reaches the initial concentration. In all cases, the stationary regime is not established.

TABLE IV

The adsorption and protective properties of iron oxides in relation to SO_2

No.	Sample*	τ' [s]	$\tau_{1/2}$ [min]	τ_{MPC} [min]	Q_{exp} ($\times 10^4$) [mol SO_2/g]
1	IS-Fe-500C	0.019	–	–	0
2	IIS-Fe-300C	0.019	–	–	0
3	IIS-Fe-500C	0.019	–	–	0.18
4	IIIS-Fe-110C	0.049	160	60	7.42
5	IVS-Fe-20C	0.069	20	–	1.06
6	IVS-Fe-110C	0.069	20	2	1.1
7	IVS-Fe-200C	0.049	230	60	9.82
8	IVS-Fe-500C	0.059	15	–	1.3
9	VS-Fe-110C	0.049	250	110	11.12
10	VS-Fe-500C	0.049	230	120	10.4

*Phase composition showed in Table II.

In Table IV generalized data characterize the kinetics of interaction of SO_2 with samples IS-Fe–VS-Fe, i.e., effective contact time of GAM with the sample (τ' [s]), SO_2 half-life ($\tau_{1/2}$ [min]), protective time of the sample (τ_{MPC} [min]), and the

specific amount of reacted sulfur dioxide (Q_{exp}). It is seen that samples VS-Fe-110 (semi-morphic mixture) and VS-Fe-500 (crystalline substance) have the best indicators (τ_{MPC}, Q_{exp}).

For the samples of the series IVS-Fe-20, IVS-Fe-110, IVS-Fe-200, and IVS-Fe-500, the effect of drying temperature on the phase composition and activity in the reaction with SO_2 can be observed.

Thus, monophasic samples IVS-Fe-20 and IVS-Fe-110 (phase α-FeO(OH)), and IVS-Fe-500 (phase α-Fe_2O_3) are inactive in the reaction with SO_2. At the same time, the sample IVS-Fe-200, which contains the phase α-FeO(OH) (78.7%) and the phase α-Fe_2O_3 (21.3%), absorbs almost 10 times more SO_2 (Table IV).

From the analysis of the data in Table IV, you can define the following series of activities:

- by time of protective action (τ_{MPC} [min]): VS-Fe-500 (120) > VS-Fe-110 (110) > IVS-Fe-200 (60) = IIIS-Fe-110 (60) ≫ IVS-Fe-110 (2);
- by the value of the specific amount of absorbed SO_2 ($Q_{exp} \times 10^4$ [mol of SO_2/g]): VS-Fe-110 (11.1) > VS-Fe-500 (10.4) > IVS-Fe-200 (9.8) > IIIS-Fe-110 (7.4) > IVS-Fe-500 (1.3) ≈ IVS-Fe-110 (1.1) ≈ IVS-Fe-20 (1.06) ≫ IIS-Fe-500 (0.18).

Samples IS-Fe-500 and IIS-Fe-300 did not absorb sulfur dioxide ($Q_{exp} = 0$).

4. Conclusions

It has been shown that the method of synthesis of iron nanooxides determines their phase composition (monophase samples of α-Fe_2O_3, γ-Fe_2O_3, and α-FeO(OH) and mixtures containing Fe_3O_4, α-FeO(OH) and γ-FeO(OH), and also α-Fe_2O_3 and α-FeO(OH) were obtained), structure, crystallite size and morphology. Testing of iron nanooxides in the reaction with sulfur dioxide in the presence of air oxygen and water vapor showed that only a semi-amorphous sample VS-Fe-110 and α-Fe_2O_3 obtained from it, and polyphase samples containing Fe_3O_4, α-FeO(OH) and γ-FeO(OH), as well as α-Fe_2O_3 and α-FeO(OH), are characterized by a protective action time (60–120 min), during which the SO_2 concentration at the reactor outlet is less than the MPC (10 mg/m^3) for the atmosphere of industrial premises.

Iron nanooxides do not catalyze the oxidation of SO_2 by atmospheric oxygen. According to XRD, SEM, and IR spectroscopy data, the interaction of SO_2 with iron nanooxides at ambient temperature leads to the formation of sulfite and bisulfite forms of adsorbed sulfur dioxide molecules.

The α-Fe_2O_3 samples obtained by thermal transformation of various precursors differ significantly in their protective properties and adsorption activity of SO_2.

References

[1] S.T. Oyama, *Cat. Rev. Sci. Eng.* **42**, 279 (2000).

[2] T. Rakitskaya, A. Truba, A. Ennan, V. Volkova, *Nanoscale Res. Lett.* **10**, 473 (2015).

[3] T.L. Rakitskaya, A.S. Truba, A.A. Ennan, V.Y. Volkova, *Adv. Mater. Res.* **1138**, 7 (2016).

[4] T.L. Rakitskaya, A.S. Truba, A.A. Ennan, V.Y. Volkova, in: *Nanostructured Materials*, Ed. J. He, Nova Science Publishers, Inc., New York 2019, p. 327.

[5] T.L. Rakitskaya, A.S. Truba, A.A. Ennan, V.N. Baumer,V.Y. Volkova, *Acta Phys. Pol. A* **133**, 1079 (2018).

[6] T. Rakitskaya, A. Truba, A. Nazar, T. Kiose, *Mol. Cryst. Liq. Cryst.* **716**, 103 (2021).

[7] J.W. Adams, D. Rodriguez, R.A. Cox, *Atmos. Chem. Phys.* **5**, 2679 (2005).

[8] G. Zhuang, Z. Yi, R.A. Duce, P.R. Brown, *Nature* **355**, 537 (1992).

[9] B.C. Faust, M.R. Hoffmann, D.W. Bahnemanni, *J. Phys. Chem.* **93**, 6371 (1989).

[10] M. Ullerstam, M.S. Johnson, R. Vogt, E. Ljungstrom, *Atmos. Chem. Phys.* **3**, 2043 (2003).

[11] J.K. Leland, A.J. Bard, *J. Phys. Chem.* **91**, 5076 (1987).

[12] X. Zhang, G. Zhuang, J. Chen, Y. Wang, X. Wang, Z. An, P. Zhang, *J. Phys. Chem. B* **110**, 12588 (2006).

[13] H. Fu, X. Wang, H. Wu, Y. Yin, J. Chen, *J. Phys. Chem. C* **111**, 6077 (2007).

[14] T. Ozkaya, M.S. Toprak, A. Baykal, H. Kavas, B. Aktaş, *J. Alloys Compd.* **472**, 18 (2009).

[15] *Handbook of Preparative Inorganic Chemistry: Six Volumes*, Vol. 5, translated from German, Ed. G. Brauer, Mir, Moscow 1985.

[16] M. Golmohammad, F. Golestanifard, A. Mirhabibi, E.M. Kelder, *Ceram. Int.* **42**, 4370 (2016).

[17] M. Gotič, G. Koščec, S. Musič, *J. Mol. Struct.* **924–926**, 347 (2009).

[18] J.V. Stark, D.G. Park, I. Lagadic, K.J. Klabunde, *Chem. Mater.* **8**, 1904 (1996).

[19] Y. Huo, Y. Zhu, J. Xie, G. Cao, T. Zhu, X. Zhao, S. Zhang, *RSC Adv.* **3**, 19097 (2013).

[20] S. Ma, Z. Wang, Y. Guo, P. Wang, Z. Yang, L. Han, J. Sun, Y. Xia, *Int. J. Nanomed.* **14**, 1051 (2019).